Adsorption of hexavalent chromium on a coal beneficiation tailing material in batch and fixed-bed column

Keila Guerra Pacheco Nunes*◉, Nathali Ribeiro Batistel◉, Dafne Lanfermann Barbosa◉, Ivan Reis Rosa◉, Ivone Vanessa Jurado Dávila◉, Liliana Amaral Féris◉

*Programa de Pós-Graduação em Engenharia Química, Universidade Federal do Rio Grande do Sul, Porto Alegre, 90035-007, Rio Grande do Sul, Brasil. *keila@enq.ufrgs.br*

Abstract

This study used a coal beneficiation tailing from Moatize (Mozambique) for the adsorption of hexavalent chromium from water in batch and fixed-bed column. Coal waste was used in a particle size between 0.7 and 1.5 mm. The effects of pH, contact time, and solid adsorbent concentration were analyzed by batch experiments. Results indicated that it was possible to obtain 98.6% removal under the experimental conditions of pH 2, 10 h contact time, and 8 g L^{-1} solid adsorbent. From these experimental results, equilibrium isotherms were built. Langmuir and Sips models presented a better fit to the experimental data. The adsorption of chromium hexavalent from aqueous solution onto coal waste was investigated in a fixed-bed column and the shape of the breakthrough curve was different in almost all of the runs, with one rate-limiting step in the adsorption, since tail formation was observed in most of the runs. The scale-up study also indicated that there is more than one rate-limiting step. Finally, the coal tailing showed important results for chromium removal in batch and fixed-bed column, indicating a potential use for the raw waste.

Keywords: Hexavalent chromium, pollutants removal, solid waste, water decontamination.

Adsorção de cromo hexavalente usando rejeito de beneficiamento de carvão em modelo de batelada e coluna de leito fixo

Resumo

Este estudo utilizou resíduo de beneficiamento de carvão de Moatize (Moçambique) para a adsorção de cromo hexavalente usando um modelo de batelada e coluna de leito fixo. O tamanho da partícula do rejeito de carvão utilizado foi entre 0,7 e 1,5 mm. Os efeitos do pH, tempo de contato e concentração de adsorvente sólido foram analisados por experimentos em batelada. Os resultados indicaram que foi possível obter 98,6% de remoção nas condições experimentais de pH 2, tempo de contato de 10 h e concentração de 8 g L^{-1} de adsorvente. A partir desses resultados experimentais, construíram-se isotermas de equilíbrio e os modelos de Langmuir e Sips apresentaram o melhor ajuste aos dados experimentais. A adsorção de cromo hexavalente em coluna de leito fixo indicou que a curva de ruptura foi diferente em quase todas os testes, com uma etapa limitante na adsorção. Finalmente, o rejeito de carvão mostrou resultados importantes para a remoção de cromo em batelada e coluna de leito fixo, exibindo uma boa utilidade para o resíduo bruto.

Palavra-chave: Cromo hexavalente, remoção de poluentes, resíduo solido, descontaminação de água.

Introduction

Coal mining is criticized for its harmful environmental impact and especially for the large-scale production and inappropriate disposal of waste and by-products that cause acid mine drainage (AMD), which has been a significant environmental problem. This problem results from the microbial oxidation of iron pyrite in presence of water and air, leading to an acidic solution that contains toxic metal ions. Heavy metal ions are a major risk to ecotoxicology and can be accumulated in living organisms (Sandeep, Vijayalatha, & Anitha, 2019).

Chromium is one of the most toxic heavy metals used in many industrial applications, being mutagenic and carcinogenic (Monteiro, Cunha, Costa, Reis, Aguiar, Oliveira-Bahia, & Rocha, 2018). The main source of water contamination with hexavalent chromium is industrial wastewater discharge (Swarnalatha, Dandaiah, Srimurali B., & Sekaran, 2008). Therefore, Cr (VI) removal from industrial effluents is fundamental and different removal techniques have already been studied to treat Cr (VI)-contaminated water (Cheng, Wang, Doudrick, & Chan, 2015).

Adsorption is an efficient method for the removal of different types of pollutants. Experiments that use a

laboratory-scale fixed-bed column of relatively large volume yield performance data can be used to design a larger pilot and industrial scale plant with high accuracy (Abdolali *et al.*, 2017).

Therefore, to minimize chromium contamination, this study used as solid adsorbent a coal tailing (R1) from Moatize (Mozambique), with adsorption in aqueous solutions in batch and fixed-bed column. The influence of several operational parameters has been analyzed (pH, contact time, solid concentration, inlet concentration, feed flow rate, and bed depth). Under the experimental results, equilibrium isotherms were built. Moreover, Langmuir and Sips models and the Bohart-Adams model were used to describe the breakthrough curves.

Materials and Methods

Chemicals and equipments

Carbon particles (size between 0.7 and 1.4 mm) were collected from a coal mine in Moatize, Mozambique. The reagents used for this study were: potassium dichromate ($K_2Cr_2O_7$, Sigma-Aldrich), sulfuric acid (H_2SO_4, anhydrous), 1,5-diphenylcarbazide ($C_{13}H_{14}N_4O$, Sigma-Aldrich), and acetone (C_3H_6O, Sigma-Aldrich).

Equipments used for this study were: pH meter (OHAUS, model Starter 3100), peristaltic pump (Ismatec MCP ISM 404B), and UV-VIS spectrophotometer (Thermo Fisher Scientific, model Genesis 10S).

Physical Characterization

The physical parameters of the coal tailing (R1) used for characterization were: specific surface area (m^2 kg^{-1}), according to the Brunauer, Emmett and Teller (BET) method; pore volume (m^3 kg^{-1}) and pore diameter (nm), using the Barrett, Joyner and Halenda (BJH) method; X-ray diffraction (XRD), carried in a D-max/2000 Rigaku X-ray diffractometer (Cu Kα radiation at 30 kV and 15 mA); X-ray fluorescence (XRF). The surface structure of the solids was analyzed with Fourier transform infrared spectroscopy (FTIR). The point of zero charge (pH_{PCZ}) was obtained by the 11-point method (Regalbuto & Robles, 2004).

Adsorption experiments

Batch adsorption experiments were carried out by adding 100 mL of 5 mg L^{-1} Cr (VI) solution, prepared with $K_2Cr_2O_7$ in distilled water. Chromium (VI) concentration was analyzed by UV-VIS at a wavelength of 540 nm, and the analysis of the Cr (VI)-1,5-diphenylcarbazide complex followed the technical standards of ASTM D5257 for hexavalent chromium determination. All experiments were made in duplicates and the removal (%) of Cr (VI) by R1 was calculated according to Equation 1.

$$Removal\ (\%) = \frac{(C_i - C_f)}{C_f} 100\% \qquad (1)$$

Where *Ci* and *Cf* are the initial and final concentrations of Cr (VI) in solution (mg L^{-1}).

Adsorption isotherm studies were carried out by varying hexavalent chromium initial concentrations from 5 to 300 mg L^{-1} under fixed conditions: 100 mL solution, pH 2, 24 h contact time, 10 g L^{-1} sorbent concentration and 298 K. Equilibrium data were analyzed by Langmuir (Equation 2), Freundlich (Equation 3), and Sips (Equation 4) models.

$$q_e = \frac{q_{máx}\ K_L\ C_e}{1 + K_L C_e} \qquad (2)$$

$$q_e = K_f\ C_e^{\frac{1}{n}} \qquad (3)$$

$$q_e = \frac{q_{máx}\ b\ C_e^{\gamma}}{1 + b\ C_e^{\gamma}} \qquad (4)$$

Where q_e is the quantity sorbed at equilibrium (mg g^{-1}); $q_{máx}$ is the maximum adsorption capacity (mg g^{-1}); K_L is the Langmuir adsorption equilibrium constant (L mg^{-1}); K_F is the Freundlich constant representing the adsorption capacity $[(mg\ g^{-1})(L\ mg^{-1})^{1/n}]$; *n* is the constant that represents the adsorption intensity (dimensionless), *b* is the equilibrium constant (L mg^{-1}), and γ is the parameter that characterizes the heterogeneity of the system.

Column Behavior

Fixed-bed experiments were carried out using a borosilicate glass column with 20 mm of internal diameter and 300 mm of total length. Coal bed length varied according to the amount of adsorbent. Hexavalent chromium solution was pumped in up-flow mode through the column at a controlled flow rate using peristaltic pump. All experiments were conducted at 298 K and at initial pH 2.

We described the fixed-bed column behavior in this study using breakthrough curves, with plots of time vs. C/C_0 (the ratio of the concentration of the solute in the column outlet at a given time t to the initial concentration of the solute in the column inlet).

The total capacity of the column ($q_{total,mg}$) provides the maximum amount of chromium that can be adsorbed by the fixed bed and can be estimated by the area under the breakthrough curve (Canteli, Carpiné, Scheer, Mafra, & Igarashi-Mafra, 2014). The total capacity of the column was calculated from Equation (5):

$$q_{total} = \frac{Q\ C_0}{1000} \int_0^{t_{sat}} \left(1 - \frac{C}{C_0}\right) dt \qquad (5)$$

Where *Q* is the column feed flow rate (mg min^{-1}), C is the outlet concentration (mg L^{-1}), C_0 is the inlet concentration (mg L^{-1}), and t_{sat} is the time required for the bed to become saturated (min.).

The bed capacity (q_{bed}, mg g^{-1}) is a parameter that determines the amount of hexavalent chromium recovered by the fixed bed per gram of adsorbent present in the bed. It was calculated from Equation (6), where m is the mass of coal present in the bed (g) (Canteli *et al.*, 2014).

$$q_{bed} = \frac{q_{total}}{m} \qquad (6)$$

Total amount of chromium (VI) fed into the column until full bed saturation (*W*) was calculated using Equation (7) (Canteli *et al.*, 2014).

$$W = \frac{Q\,C_0\,t_{sat}}{10^3} \qquad (7)$$

The bed behavior (*P*) relates the amount of hexavalent chromium retained in the bed (q total) with the amount of chromium fed in the same run (*W*) (Scheer *et al.*, 2014). High performance indicates a good operational set up. The performance was calculated using Equation (8):

$$P(\%) = \frac{q_{total}}{W}\,100\% \qquad (8)$$

Adsorbent utilization (ŋ) relates the total capacity obtained in the fixed bed (q$_{bed}$) with the total capacity obtained in a batch expeg1riment (q$_{batch}$) and therefore represents the amount of active sites that are not utilized in the fixed bed. This parameter was calculated from Equation (9).

$$ŋ = \frac{q_{bed}}{q_{batch}} \qquad (9)$$

The residence time, which affects the breakthrough curve, is the time required for the fluid to fill the empty column. The true residence time (TRV) was calculated from Equation (10).

$$TRV = \frac{\varepsilon\,V_L}{Q} \qquad (10)$$

Where ε is the bed porosity and V_L is the volume occupied by the adsorbent inside the bed (mL). The bed porosity can be estimated by the fraction of empty spaces (volume of distilled water present in the fixed bed after packing (mL) divided by the fixed bed volume (mL).

Scale-up study

The bed depth service time (BDST) model was studied to predict the relationship between bed depth, *Z* (cm), and operation time, *t* (min). Equation (11) expresses a linear relationship between bed depth and service time (Zou, Zhao, & Zhu, 2013).

$$t = \frac{N_0}{C_0}Z + \frac{1}{K_{BDST}\,C_0}\,In\left(\frac{C_0}{C_t} - 1\right) \qquad (11)$$

here N_0 is the adsorption capacity (mg mL^{-1}), v is the fluid velocity (cm min^{-1}), C_t is the outlet concentration at time t (mg mL^{-1}), and K$_{BDST}$ is the mass transfer coefficient (mL mg^{-1} min^{-1}). K$_{BDST}$ and N$_0$ can be calculated from the linear and angular coefficient, respectively, from the graph of *t* as a function of *Z* at a given C_t/C_0 ratio (iso-concentration line). At 50% breakthrough ($C_t/C_0 = 0.50$ and t = t$_{0.50}$), the linear term of Equation (11) becomes indeterminate (ln(1)), and the equation is thus reduced to Equation (12):

$$t_{0,50}\frac{N_0}{C_0 v}Z \qquad (12)$$

The graph of t$_{0.50}$ at 50% breakthrough as a function of *Z* forms a line passing through the origin, and N_0 was calculated by the angular coefficient.

Results and discussion

Characterization

The physical characterization of coal reject reported the following values:,Surface area (2724 m^2 kg^{-1}), Pore volume (6 10^{-6} m^3 kg^{-1}), Pore diameter (3.32 nm), pH$_{PZC}$ (5.4). This pore diameter classifies the coal as mesoporous. This characteristic of the solid adsorbents is a favorable structural property for removing large molecules.

The diffractogram shows that the main minerals found in the carbon wastes were quartz, kaolinite, hematite, gypsum, and dolomite (Figure 1). The XRD profile is aligned with the XRF results (Table 1), were it can be seen the high contents of silica in the quartz, alumina in the kaolinite, and iron oxide in the hematite. The results are similar to those reported in the literature (Duarte *et al.*, 2018; M. L. S. Oliveira *et al.*, 2018).

The X-ray diffraction analysis for raw coal tailing and coal tailing after chromium adsorption is also presented in Figure 1. This figure shows that after adsorption the sample is less crystalline, with decreased packing intensity, being implied that hexavalent chromium ions were replacing coal tailing ions and altering the structure (surface) of the solid.
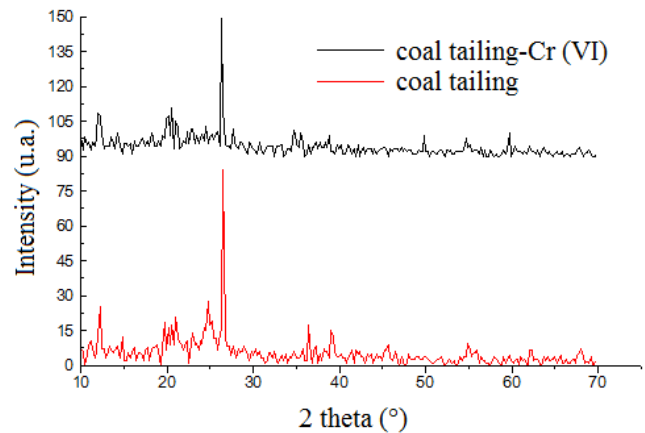

Figure 1. X-ray patterns of coal waste before and after chromium adsorption. Conditions: pH 2, initial concentration of 8 g L-1, contact time of 10 h.

Table 1. X-ray fluorescence analysis results coal reject before chromium adsorption.

Composition	Level (%)	Composition	Level (%)
SiO$_2$	24.29	TiO$_2$	0.68
Al$_2$O$_3$	9.98	K$_2$O	0.58
Fe$_2$O$_3$	3.16	P$_2$O$_5$	0.36
SO$_3$	2.83	MgO	0.24
CaO	1.44	Cr$_2$O$_3$	0.02
Others			0.06
Loss on ignition (1273 K)			56.36

The principal elements observed in the surface coal tailing sample were Si, Al, Fe, C, O, and Ti (Figure 2), whose composition is shown in Table 1.

The FTIR spectrums that exhibit a similar trend between coal tailing before and after chromium adsorption (Figure 3). The band at about 3650 cm^{-1} can be assigned to the stretching vibration of the octahedral OH$^-$ group. The bands at about

1500-1700 cm^{-1} can be associated to aliphatic amino (NH) and aliphatic alkyl groups. Bands in the range of 900 to 1050 cm^{-1} indicate the presence of iron sulfates, aliphatic alcohol, and ether groups. The peaks in about 600-700 cm^{-1} are characteristic of S-S bonds.
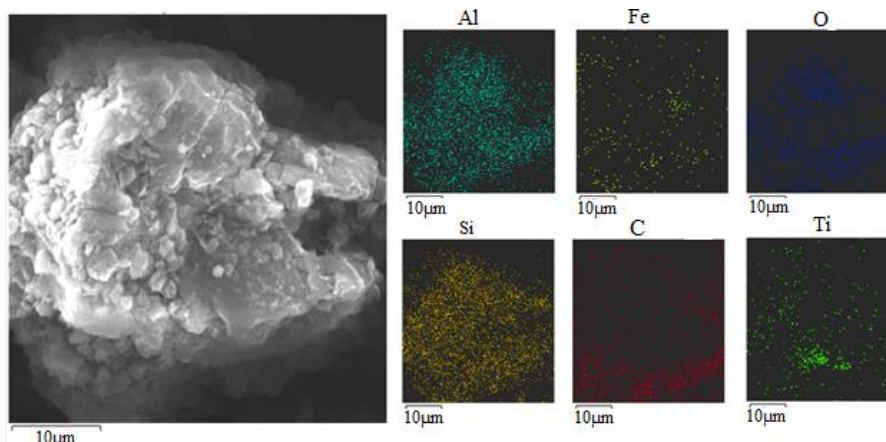

Figure 2. Scanning electron microscope with energy dispersive spectroscopy images for a coal tailing sample.

These results are similar to those reported in the literature. Oliveira, Machado, Duarte, & Peterson (2016) investigated a coal mine and found similar results for the FTIR spectrum. Bands at 900–1200 cm^{-1} were found, showing the presence of sulfates. Maass, Valério, Lourenço, de Oliveira, & Hotza (2019) studied the FTIR spectra of mineral coal tailings and found similar bands (about 1143 cm^{-1}), which were associated to alcohols, acetate, ethers, and carboxyl compounds. Bands in the range of 900 to 1200 cm^{-1} are associated to the presence of iron sulfates, and peaks at 490, 594, 673 cm^{-1} are characteristic of S-S bonds.

Also, in FTIR analysis; the reduction of principal bands may indicate the substitution of ions of the solid by chromium (VI) ions, which suggests interaction between surface groups present on the coal tailing and chromium. However, characteristic bands may be overlapped by some other bands thus hindering detection.
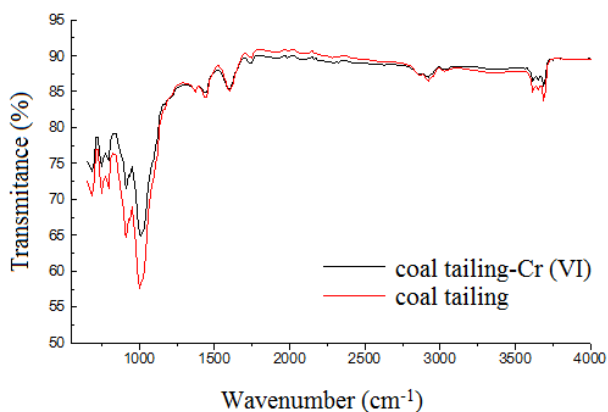

Figure 3. FTIR spectrums before and after chromium adsorption. Conditions: pH 2, initial concentration of 8 g L^{-1}, contact time of 10 h.

Ideal adsorption conditions

Cr (VI) adsorption was significantly affected by pH variation, with the best results being found at the lowest pH (Figure 4). Maximum chromium removal was about 27%, at pH 2. For this reason, this parameter was fixed in proximal experiments. Chromium (VI) removal at acidic pH when alternative adsorbents are used has been reported in others studies. Dehghani, Sanaei, Ali, & Bhatnagar (2016) studied chromium (VI) removal from aqueous solution using treated waste newspaper as adsorbent and found the process to be highly pH-dependent, with high removal at acidic pH (3). Koloczek, Jarosław, & Zukowski (2015) investigated peat and coconut fiber as biofilters for chromium adsorption from contaminated wastewater and also found maximum adsorption capacity at acidic pH (1.5).

The solution pH is an important parameter in the adsorption process as it affects the adsorbent surface charge and the Cr (VI) ionic form. In aqueous solution, Cr (VI) exists in different forms according to the pH and its concentration in aqueous solution. At pH 2 and initial Cr (VI) concentration of 5 mg L^{-1}, the dominant species is hydrogenchromate (HCrO$_4^-$). The adsorbent surface charge can be predicted through the zero charge point. The surface has a positive charge at pH below the PCZ, and a negative charge at pH above the PCZ. In the aforementioned conditions, the adsorbent surface is thus positively charged, once pH 2 is lower than the pH$_{PCZ}$ of the solid (pH$_{PCZ}$ = 5.4). Chromium (VI) being in an anionic form and the adsorbent surface being positively charged increase their electrostatic attraction, therefore increasing Cr (VI) removal from the aqueous solution.

Figure 4A shows that with an increase in contact time, Cr (VI) removal also increases until baseline, where the equilibrium is arrived. This baseline indicates that over time the active sites in the adsorbent surface are being occupied until the solid saturation point is reached and all sites are filled. Chromium (VI) adsorption reached the equilibrium after 10 h, and 99.5% of chromium was removed with a residual concentration of 0.03 mg L^{-1} in solution. The notable difference between the maximum adsorption times for the solids indicates that the process is controlled by the surface, meaning that the adsorbent surface area is an important parameter for this process.

Figure 4C shows that Cr (VI) removal increased with the increase of adsorbent concentration in solution. This growth is related with the growth of the adsorbent superficial area, explaining the high values in available active sites. The maximum point for chromium removal was found to be 8 g L^{-1} coal waste. After this concentration a saturation phase is reached, where approximately 99% of Cr (VI) was removed from the aqueous solution and the solid was saturated, therefore leading to the residual Cr (VI) concentration of 0.07 mg L^{-1} in the solution.

The results obtained so far show that the best conditions for Cr (VI) sorption onto coal waste were: solution pH = 2, contact time = 10 h, and adsorbent dosage = 8 g L^{-1}.
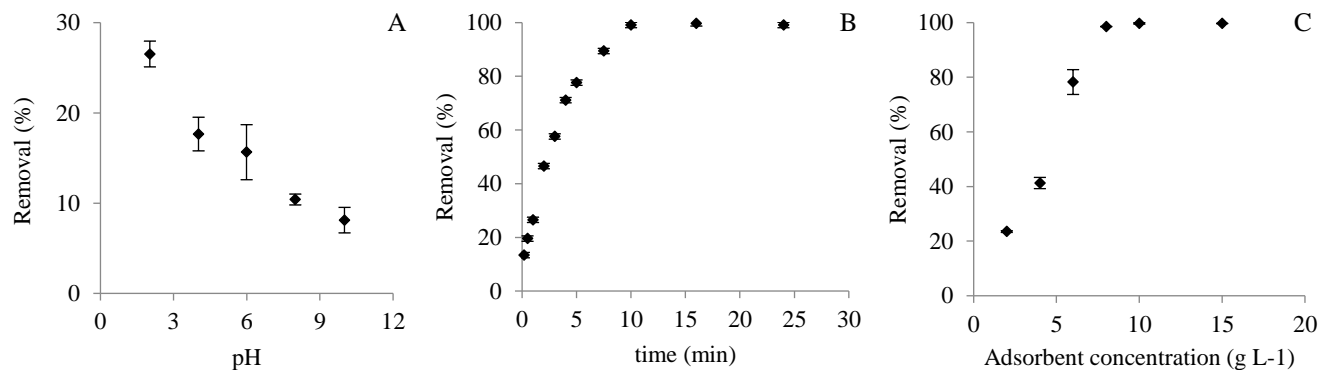

Figure 4. Effect of the variation of (A) solution pH, (B) contact time, and (C) solid concentration on Cr (VI) removal per coal waste.

Adsorption isotherms

The experimental data presented a better fit to Langmuir and Sips models (Figure 5), with an R^2 = 0.90 (Table 2). Sips model also presented a good fit, with a correlation coefficient equal to the Langmuir model. This can be explained by the Sips γ parameter, which indicates the adsorbent surface heterogeneity. When γ is closer to the unity, the less heterogenic is the surface, and when γ=1 Sips model reduces to the Langmuir model. In this case, the coal with γ=0.89 explains why Sips and Langmuir correlation coefficients are similar.

parameter q$_{max}$ is 2.64 mg of Cr (VI) per gram of adsorbent, and Sips q$_{max}$ is 2.69 mg of Cr (VI) per gram of adsorbent.

The results obtained were similar to those reported in the literature regarding chromium (VI) removal on different solid adsorbents. Samuel *et al.* (2019) investigated the adsorption of hexavalent chromium using chitosan grafted graphene oxide (CS-GO) nanocomposite in batch mode. The adsorption capacity of 104.16 mg g^{-1} was achieved at pH 2.0 and contact time of 420 min. The adsorption process was described by the Langmuir isotherm model.

Table 2. Parameters for the isotherms to Langmuir, Freundlich, and Sips models for chromium adsorption on coal waste.

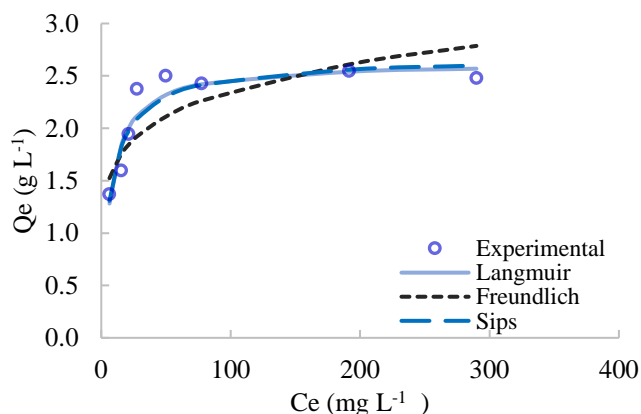| Parameter	Langmuir	Freundlich	Sips
q$_{max}$	2.64	-	2.69
K$_L$	0.14	-	-
K$_F$	-	1.13	-
K$_S$	-	-	0.18
n	-	6.27	-
γ	-	-	0.89
R^2	0.90	0.74	0.90

Figure 5. Comparison between the isotherm experimental data and the values predicted by the three models, where Ce is ion concentration in equilibrium and Qe is quantity sorbed at equilibrium. (Experiment conditions: solution volume of 100 mL, pH 2, and adsorbent dosage of 8 g L^{-1}).

The Langmuir and Sips baselines correspond to the maximum adsorption capacity (q$_{max}$) where the adsorbent reaches saturation and all active sites are filled. The Langmuir

Column study

In previous results, the total capacity of the adsorbent coal obtained from batch studies (q$_{batch}$) was 2.723 mg g^{-1}, which was used to obtain the ŋ values in the column study. Table 3 shows that total column capacity (q$_{total}$) and bed capacity (q$_{bed}$) increase when inlet concentrations increase (between 3 and 6.5 ppm). However, this does not happen at 10 ppm, since t$_{rup}$ is very short. Bed performance, P (%), becomes slightly higher at high concentrations, and the breakthrough time (t$_{sat}$) is lower when the inlet concentration

increases.

Lower concentration gradients cause the transport within the pores to occur slowly due to reductions in the coefficients of diffusion and/or mass transfer, which results in an increase in the saturation time. P (%) increases as C_0 increases. The values of q_{bed}, q_{total}, and ŋ were very similar at higher C_0.

The change in the initial metal ion concentration has a significant effect on the breakthrough curve as illustrated in Figure 6A. The larger the initial feed concentration, the steeper is the slope of the breakthrough curve and the smaller is the breakthrough time. These results demonstrate that the change of concentration gradient affects the saturation rate and breakthrough time; in other words, the diffusion process is concentration-dependent. As the feed concentration increases, the metal loading rate increases, but so does the driving force for mass transfer, which culminate in a decrease in the adsorption zone length (Chen *et al.*, 2012).

The adsorption efficiency is higher at lower flow rates (Figure 6B). This can be explained by the fact that at lower flow rates, the residence time of the adsorbate is longer and hence the adsorbent gets more time to bond with the metal efficiently. In other words, if the residence time of the solute in the column is not long enough for adsorption equilibrium to be reached at the given flow rate, the Cr (VI) solution leaves the column before equilibrium occurs.

Table 3. Comparison of coal waste fixed-bed performance for chromium VI adsorption under different inlet concentrations (C_0, ppm), feed flow rates (Q, mL.min^{-1}), and bed depth (Z, mm).

C_0	TRV (sec)	q_{bed} (mg g^{-1})	q_{total} (mg)	ŋ (%)	W (g)	P (%)	t_{rup} (min)	t_{sat} (min)
3	0.3	0.17	0.52	6	1.8	29	21	120
6.5	0.3	0.30	0.91	11	2.9	31	15	90
10	0.3	0.26	0.79	10	2.0	40	8	40
Q	TRV	q_{bed}	q_{total}	ŋ	W	P	t_{rup}	t_{sat}
5	0.3	0.29	0.89	11%	2.0	45	8	40
10	0.2	0.27	0.82	10%	2.0	41	8	20
15	0.1	0.25	0.75	9%	1.5	50	4	10
Z	TRV	q_{bed}	q_{total}	ŋ	W	P	t_{rup}	t_{sat}
7	0.2	0.32	0.95	12	2.5	38	6	25
16	0.9	0.15	1.0	5	3.0	32	8	30
30	3.2	0.22	2.6	8	12.0	21	9	120

C_0: initial concentration of chromium, TRV: true residence time, q_{bed}: bed capacity, q_{total}: total column capacity, ŋ: relation of adsorbent, W: total quantity of adsorbate in the column, P: bed performance, t_{rup}: breakthrough time, and t_{sat}: saturation time.

The parameters calculated reported that t_{sat}, q_{bed}, q_{total}, and ŋ decrease as Q increases (Table 3). Is addition, when Q increases, TRV decreased, which causes a negative effect on the mass transfer efficiency, thus resulting in a decreased t_{sat}.

These breakthrough curves show the efficiency of the process. It was also observed that adsorbent gets saturated easily at higher flow rates. As shown in Table 3, saturation occurred at 40, 20, and 10 min with flow rates of 5, 10, and 15 mL min^{-1}, and the respective residence times were 0.3, 0.2, and 0.1 s. With higher residence time, Cr (VI) ions had more

time to be in contact with the adsorbent, which resulted in greater removal of Cr (VI) ions in the fixed-bed column.
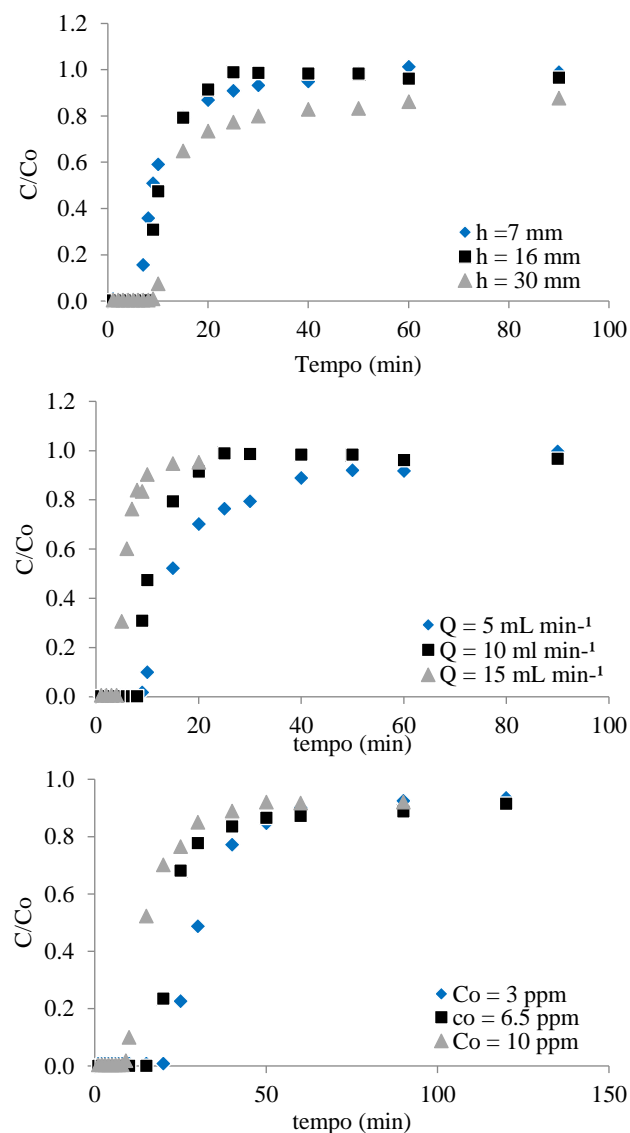

Figure 6. Curves obtained with varied (A) inlet concentrations (C_0), (B) feed flow rates (Q), and (C) bed depth of experimental breakthrough curves for chromium VI onto coal-packed column at T = 293 K and D = 20 mm.

According to Ko, Porter, & McKay (2001), an increase in the feed flow changes the diffusion of the film without changing intraparticle diffusion. The movement of the adsorbate from the solution to the region surrounding the adsorbent causes a concentration gradient to develop at this interface, which allows the adsorbate to cross over the film and be adsorbed. In addition, an increase in the solution velocity reduces the adhesion of the adsorbate to the adsorbent and consequently reduces the efficiency of the process (Tan, Ahmad, & Hameed, 2008) .

The P (%) values obtained for flow rates equal to 5 and 15 mL min^{-1} were similar; however the P (%) values obtained for the highest flow rate was 50%. This result may be explained by the little amount of adsorbate fed into the

bed (W) to reach bed saturation.

Figure 6C shows the effect of changing the bed depth (Z) between 7 and 30 mm. Data are shown in Table 3. The other parameters remained constant.

As Z increases, t_{sat} and q_{total} also increase as a result of the higher number of available active sites. Moreover, the total surface area also increases, consequently increasing the adsorbent mass (Scheer *et al*., 2014).

As Z increases, P decreases, this result may have occurred because of the tail formed at higher bed depths. The increase in the tail implies a higher Cr (VI) loss, which reduces the column performance. An inverse relationship between *h* and P was observed. As the adsorbent becomes saturated, more adsorbate is consumed.

Conclusion

The best conditions for Cr (VI) adsorption were found at 8 g L^{-1} adsorbent dosage (pH 2, 10h). The isotherms obtained fitted both Langmuir and Sips models, indicating that adsorption occurs at homogeneous sites and forms a monolayer. When compared with other adsorbents found in the literature regarding Cr (VI) adsorption, the coal tailings studied did not present the best adsorption capacities. However, is important to remember that coal tailing is a low-cost waste material that can be found in abundance and was used raw, without any previous treatment. The shape of the breakthrough curve was different in almost all of the runs. Additionally, it can be found that there is more than one rate-limiting step in the adsorption of hexavalent chromium onto coal, since tail formation was observed in most of the runs. The scale-up study also showed this finding. The BDST model was applied to the experimental data and used for the scale-up study, demonstrating that this model is suitable for scaling up the system.

References

Abdolali, A., Ngo, H. H., Guo, W., Zhou, J. L., Zhang, J., Liang, S., & Liu, Y. (2017). Application of a breakthrough biosorbent for removing heavy metalsfrom synthetic and real wastewaters in a lab − scale continuous A continuous fixed − bed study was carried out utilising a breakthrough biosorbent. *Bioresource Technology*, *229*, 78–87. doi: 10.1016/j.biortech.2017.01.016

Acheampong, M. A., Pakshirajan, K., Annachhatre, A. P., & Lens, P. N. L. (2013). Removal of Cu (II) by biosorption onto coconut shell in fixed-bed column systems. *Journal of Industrial and Engineering Chemistry* *19*(3), 841–848. doi: 10.1016/j.jiec.2012.10.029

Canteli, A. M. D., Carpiné, D., Scheer, A. de P., Mafra, M. R., & Igarashi-Mafra, L. (2014). Fixed-bed column adsorption of the coffee aroma compound benzaldehyde from aqueous solution onto granular activated carbon from coconut husk. *LWT - Food Science and Technology*, *59*(2P1), 1025–1032. doi:10.1016/j.lwt.2014.06.015

Chen, S., Yue, Q., Gao, B., Li, Q., Xu, X., & Fu, K. (2012). Adsorption of hexavalent chromium from aqueous solution by modified corn stalk : A fixed-bed column study. *Bioresource Technology*, 113, 114–120. doi:10.1016/j.biortech.2011.11.110

Cheng, Q., Wang, C., Doudrick, K., & Chan, C. K. (2015). Hexavalent chromium removal using metal oxide photocatalysts. *Applied Catalysis B: Environmental*, 176–177, 740–748. doi:10.1016/j.apcatb.2015.04.047

Dehghani, M. H., Sanaei, D., Ali, I., & Bhatnagar, A. (2016). Removal of chromium(VI) from aqueous solution using treated waste newspaper as a low-cost adsorbent: Kinetic modeling and isotherm studies. *Journal of Molecular Liquids*, 215, 671–679. doi:10.1016/j.molliq.2015.12.057

Duarte, A. L., DaBoit, K., Oliveira, M. L. S., Teixeira, E. C., Schneider, I. L.,

& Silva, L. F. O. (2018). Hazardous elements and amorphous nanoparticles in historical estuary coal mining area. *Geoscience Frontiers*, *10*(3), 927-939. doi:10.1016/j.gsf.2018.05.005

Ko, D. C. K., Porter, J. F., & McKay, G. (2001). Film-pore diffusion model for the fixed-bed sorption of copper and cadmium ions onto bone char. *Water Research*, *35*(16), 3876–3886. doi:10.1016/S0043-1354(01)00114-2

Koloczek, H., Jarosław, C., & Zukowski, W. (2015). *Peat and coconut fiber as biofilters for chromium adsorption from contaminated wastewaters. Environmental Science and Pollution Research*, *23*(1), 527-534. Recovered from https://link.springer.com/article/10.1007%2Fs11356-015-5285-x

Kundu, S., & Gupta, A. K. (2007). As(III) removal from aqueous medium in fixed bed using iron oxide-coated cement (IOCC): Experimental and modeling studies. *Chemical Engineering Journal*, *129*(1–3), 123–131. doi:10.1016/j.cej.2006.10.014

Maass, D., Valério, A., Lourenço, L. A., de Oliveira, D., & Hotza, D. (2019). Biosynthesis of iron oxide nanoparticles from mineral coal tailings in a stirred tank reactor. *Hydrometallurgy*, 184, 199–205. doi:10.1016/j.hydromet.2019.01.010

Oliveira, C. M., Machado, C. M., Duarte, G. W., & Peterson, M. (2016). Beneficiation of pyrite from coal mining. *Journal of Cleaner Production*, 139, 821–827. doi:10.1016/j.jclepro.2016.08.124

Oliveira, M. L. S., Da Boit, K., Schneider, I. L., Teixeira, E. C., Crissien Borrero, T. J., & Silva, L. F. O. (2018). Study of coal cleaning rejects by FIB and sample preparation for HR-TEM: Mineral surface chemistry and nanoparticle-aggregation control for health studies. *Journal of Cleaner Production*, 188, 662–669. doi:10.1016/j.jclepro.2018.04.050

Samuel, M. S., Bhattacharya, J., Raj, S., Santhanam, N., Singh, H., & Pradeep Singh, N. D. (2019). Efficient removal of Chromium(VI) from aqueous solution using chitosan grafted graphene oxide (CS-GO) nanocomposite. *International Journal of Biological Macromolecules*, 121, 285–292. doi:10.1016/j.ijbiomac.2018.09.170

Sandeep, G., Vijayalatha, K.R., Anitha, T. (2019) Heavy metals and its impact in vegetable crops. Int. J. Chem. Stud., *7*(1), pp. 1612-1621.

Scheer, A. D. P., Mafra, M. R., Marcos, A., Canteli, D., Carpin, D., & Igarashi-mafra, L. (2014). Fixed-bed column adsorption of the coffee aroma compound benzaldehyde from aqueous solution onto granular activated carbon from coconut husk. *LWT - Food Science and Technology*, *59*(2), 1025-1032. doi:10.1016/j.lwt.2014.06.015

Singh, T. S., & Pant, K. K. (2006). Experimental and modelling studies on fixed bed adsorption of As(III) ions from aqueous solution. *Separation and Purification Technology*, *48*(3), 288–296. doi:10.1016/j.seppur.2005.07.035

Swarnalatha, S., Dandaiah, S., Srimurali b, M., & Sekaran, G. (2008). Safe disposal of toxic chrome buffing dust generated from leather industries. *Journal of Hazardous Materials* 150(2) 290–299. doi:10.1016/j.jhazmat.2007.04.100

Tan, I. A. W., Ahmad, A. L., & Hameed, B. H. (2008). Adsorption of basic dye using activated carbon prepared from oil palm shell: batch and fixed bed studies. *Desalination*, *225*(1–3), 13–28. doi:10.1016/j.desal.2007.07.005

Zou, W., Zhao, L., & Zhu, L. (2013). Adsorption of uranium(VI) by grapefruit peel in a fixed-bed column: Experiments and prediction of breakthrough curves. *Journal of Radioanalytical and Nuclear Chemistry*, *295*(1), 717–727. Recovered from https://link.springer.com/article/10.1007%2Fs10967-012-1950-4